

# Inhibitor of Apoptosis Proteins Determine Glioblastoma Stem-Like Cells Fate in an Oxygen-Dependent Manner

AURÉLIE SOUBÉРАН,<sup>a</sup> JESSICA CAPPAÏ,<sup>a</sup> MATHIEU CHOCRY,<sup>a</sup> CHRISTOPHER NUCCIO,<sup>b</sup> JULIE RAUJOL,<sup>c</sup> CAROLE COLIN,<sup>a</sup> DANIEL LAFITTE,<sup>b</sup> HERVÉ KOVACIC,<sup>a</sup> VÉRONIQUE QUILLIEN,<sup>d,e</sup> NATHALIE BAEZA-KALLEE,<sup>a</sup> GENEVIÈVE ROUGON,<sup>f</sup> DOMINIQUE FIGARELLA-BRANGER,<sup>a,g</sup> AURÉLIE TCHOGHANDJIAN <sup>a</sup>

**Key Words.** Glioblastoma stem-like cells • Hypoxia • IAP proteins • ATR • TNF $\alpha$

<sup>a</sup>Aix-Marseille University, CNRS, INP, Institute of NeuroPhysiopathology, Marseille, France; <sup>b</sup>Aix-Marseille University, INSERM UMR MD1, Marseille, France; <sup>c</sup>Tescan Analytic SAS, Fuveau, France; <sup>d</sup>Rennes 1 University, “Chemistry, Oncogenesis, Stress, Signaling”, INSERM U1242, Rennes, France; <sup>e</sup>Centre de lutte contre le cancer Eugène Marquis, Rennes F-35042, France; <sup>f</sup>Aix-Marseille University, Institut de Neurosciences Timone, CNRS 7289, Marseille, France; <sup>g</sup>AP-HM, Timone Hospital, Department of Anatomopathology, Marseille, France

Correspondence: Aurélie Tchoghandjian, Ph.D., INP, Institute of NeuroPhysiopathology, CNRS UMR 7051, 13385 Marseille Cedex 05, France. Telephone: 04-91-32-44-43; e-mail: aurelie.tchoghandjian@univ-amu.fr

Received June 22, 2018; accepted for publication February 11, 2019; first published online in *STEM CELLS EXPRESS* March 28, 2019.

<http://dx.doi.org/10.1002/stem.2997>

## ABSTRACT

In glioblastomas, apoptosis inhibitor proteins (IAPs) are involved in apoptotic and non-apoptotic processes. We previously showed that IAPs inhibition induced a loss of stemness and glioblastoma stem cells differentiation by activating nuclear factor- $\kappa$ B under normoxic conditions. Hypoxia has been shown to modulate drug efficacy. Here, we investigated how IAPs participate in glioblastoma stem-like cell maintenance and fate under hypoxia. We showed that in a hypoxic environment, IAPs inhibition by GDC-0152, a small-molecule IAPs inhibitor, triggered stem-like cell apoptosis and decreased proliferation in four human glioblastoma cell lines. We set up a three-dimensional glioblastoma spheroid model in which time-of-flight secondary ion mass spectrometry analyses revealed a decrease in oxygen levels between the periphery and core. We observed low proliferative and apoptotic cells located close to the hypoxic core of the spheres and glial fibrillary acidic protein<sup>+</sup> cells at their periphery. These oxygen-dependent GDC-0152 antitumoral effects have been confirmed on human glioblastoma explants. Notably, serine–threonine kinase activation analysis revealed that under hypoxic conditions, IAPs inhibition activated ataxia telangiectasia and Rad3-related protein signaling. Our findings provide new insights into the dual mechanism of action of IAPs inhibitors that depends on oxygen level and are relevant to their therapeutic application in tumors. *STEM CELLS* 2019;00:1–12

## SIGNIFICANCE STATEMENT

Glioblastomas are highly aggressive and hypoxic tumors. To improve treatment efficiency, it is essential to get rid of cancer stem-cells. One challenge is to target glioblastoma stem-like cells localized in hypoxic areas as this environment maintains stem cells properties and contributes to treatment resistance. This study found that pharmacological inhibition of inhibitor of apoptosis proteins by Smac mimetic GDC-0152 was able to decrease glioblastoma stem-like cells viability in hypoxia by decreasing cell proliferation and increasing apoptosis through ATR and TNF $\alpha$  pathways.

## INTRODUCTION

Glioblastomas (GBMs) are highly aggressive, infiltrative, hypoxic brain tumors. Numerous studies have shown that GBMs are derived from cancer stem cells. Targeting GBM stem cells, which drive relapses and participate in resistance to treatment, are a major challenge in efforts to improve overall survival of patients. These GBM stem cells are often located close to hypoxic areas that maintain their self-renewal properties [1], an environment that might also influence cell drug responses. GBM stem cells are characterized by cell surface antigens, such as CD133 [2] or, as we have shown, gangliosides recognized by A2B5 antibody [3]. A2B5<sup>+</sup> GBM cells harbor stem-like cell properties as evidenced by their ability to

self-renew to form spheres, proliferate, and differentiate in vitro and initiate a tumor similar to the parental one in vivo [4, 5].

In cancer cells, inhibitor of apoptosis proteins (IAPs) are often overexpressed and inhibit caspases activation and apoptosis and therefore contribute to treatment resistance [6]. In addition to controlling programmed cell death, IAPs regulate mitogen-activated protein kinase (MAPK) as well as both canonical and non-canonical nuclear factor- $\kappa$ B (NF- $\kappa$ B) pathways [7–11] leading to the transcription of target genes, such as tumor necrosis factor  $\alpha$  (TNF $\alpha$ ) [12–14]. IAPs expression level can be regulated by small molecules that mimic the N-terminal of second mitochondria-derived activator of caspase (Smac), an endogenous IAPs antagonist.

In a previous study, we used the Smac mimetic GDC-0152, which antagonizes cIAP1, cIAP2, XIAP, and ML-IAP [15] to test for its antitumoral activity in GBMs [16]. GDC-0152 treatment increased survival of mice xenografted with U87-MG GBM cells, whereas cultured GBM stem-like cells were more resistant to GDC-0152-induced cell death [16]. We then explored whether IAPs inhibition could affect the fate of GBM stem-like cells. We found that in normoxia, IAPs inhibition by Smac mimetics triggered GBM stem-like cells differentiation by activating the NF- $\kappa$ B pathway [17].

In the present study, because hypoxia has been shown to modulate drug efficacy and IAPs expression, we investigated whether oxygen level could modify GBM stem-like cell fate upon IAPs inhibition [18–20]. To this end, we first investigated IAPs expression in human GBMs and then investigated the effect of their inhibition by the Smac mimetic GDC-0152 on GBM stem-like cell differentiation, viability, proliferation, and death under hypoxic and normoxic conditions.

## MATERIALS AND METHODS

### Immunohistochemistry

After steam-heat-induced antigen retrieval, 5- $\mu$ m sections of formalin-fixed paraffin-embedded samples were tested for the presence of cIAP1 (AF8181, R&D Systems, Wiesbaden, Germany), cIAP2 (AF8171, R&D Systems), XIAP (clone 48, BD Biosciences, Franklin Lake, NJ), ML-IAP (IMG-347A, Imegenex, Cambridge, U.K.), carbonic anhydrase IX (CAIX; GTX15086, GeneTex, Inc., Irvine). A Benchmark Ventana autostainer (Ventana Medical Systems, Tucson, AZ, USA) was used for detection, and slides were simultaneously immunostained to avoid intermanipulation variability. Slides were then scanned (Nanozoomer 2.0-HT, Hamamatsu Photonics SARL France, Massy, France) and images processed in NDP.view2 software (Hamamatsu).

### Microarray Data Source

Expression profile by microarrays was obtained from National Center for Biotechnology Information Gene Expression Omnibus (NCBI GEO, <http://www.ncbi.nlm.nih.gov/geo/>) [21, 22]. We downloaded and reanalyzed the raw data of a previous Affymetrix Human Genome U133 Plus 2.0 Array (GDS1380/GSE2485) study that investigated molecules differentially expressed in laser capture microdissected peri-necrotic palisades versus other GBM tumor area [23]. We focused on the differential transcriptomic expression profiles of cIAP1 (202076\_at), cIAP2 (210538\_s\_at), XIAP (206536\_s\_at), and ML-IAP (220451\_s\_at) in these two groups of samples.

### Cell Lines and Reagents

Four primary GBM stem-like cell lines were used. GBM6, GBM9, and GBM40 were isolated from different human GBMs and derived from A2B5<sup>+</sup> cells [5] and RNS175 was isolated from human GBM without any selection. All these cell lines are *IDH*<sup>wt</sup>. According to Verhaak classification [24, 25], GBM6 and RNS175 were classified as mesenchymal cell lines, GBM9 as proneural cell line and GBM40 as classic cell line [5]. These cells were grown as floating spheres in serum-free medium supplemented with epidermal growth factor (EGF), basic fibroblast growth factor (bFGF), and B27 [4]. Smac mimetic GDC-0152 was purchased from Selleckchem (Write Houston, TX, USA) and Ataxia Telangiectasia and Rad3 (ATR) inhibitor from Merck KGaA (Darmstadt, Germany) (ATR inhibitor

[ATRI] III; ETP-46464, Darmstadt, Germany). TNF $\alpha$  blocking antibody Enbrel (Pfizer, NY) was kindly provided by S. Guis. For GDC-0152 treatment experiments, cells were grown either as spheres in suspension or as monolayers on 10  $\mu$ g/ml poly-DL-ornithine (Sigma-Aldrich, St. Louis, MO, USA) coated dishes. Spheres were treated after 8 days of culture for 8 days, whereas cells cultivated as monolayer on 10  $\mu$ g/ml poly-DL-ornithine (Sigma-Aldrich) were treated after 24 hours for 8 days. All the cell lines were grown at 37°C in a humidified atmosphere of 5% CO<sub>2</sub> and 95% air including 20% O<sub>2</sub> for normoxic condition or in a humidified atmosphere of 5% CO<sub>2</sub> and 2% O<sub>2</sub> supplemented with nitrogen (trigaz incubator O<sub>2</sub>-N<sub>2</sub>-CO<sub>2</sub>, Sanyo, Osaka, Japan) for hypoxic condition.

### Self-Renewal Analysis

After 24 hours, cells cultivated in monolayer were treated with 1 nM of GDC-0152 or dimethyl sulfoxide (DMSO) for 8 days. At the end of treatment, the supernatant was removed, cells were harvested, dissociated into single cells, and plated in 96-well plates (1–5 cells per well) with serum-free medium supplemented with EGF, bFGF, and B27. Eight days later, the number of spheres was counted and divided by the original number of cells seeded to evaluate the sphere formation property.

### Spheres Diameter Measurement

Cells were grown as floating spheres for 8 days and then treated with 1  $\mu$ M of GDC-0152 or DMSO for 8 days. At the endpoint, size of spheres were assessed using a  $\times$ 10 magnification and a calibrated micrometer reticule on Leica microscope (Wetzlar, Germany; 1 division = 11.8  $\mu$ m).

### Explant Cultures of Human GBM Tissue

Ten GBMs tissue samples were collected after surgery and placed in Dulbecco's modified Eagle's medium (DMEM) supplemented with 0.5% fetal calf serum (FCS), 1% penicillin–streptomycin, and 1% sodium pyruvate (Gibco-Invitrogen, Cergy Pontoise, France). Tissues were cut into 500  $\mu$ m pieces in DMEM + 10% FCS, and plated on 12-well plates or labtek chambers (BD Biosciences) pre-coated with poly-(L)-lysine (10  $\mu$ g/ml; Sigma-Aldrich). Medium was supplemented with 0.4% methylcellulose (Sigma-Aldrich). Explant cultures were then incubated at 37°C in a humidified atmosphere of 5% CO<sub>2</sub> and 95% air including 20% O<sub>2</sub> for normoxic condition or in a humidified atmosphere of 5% CO<sub>2</sub> and 2% O<sub>2</sub> supplemented with nitrogen for hypoxic condition. After 72 hours of culture, explants were treated with 1  $\mu$ M of GDC-0152. After 72 hours of treatment, explants were processed for flow cytometry and immunohistochemistry experiments.

### Reverse-Transcription, Real-Time Quantitative PCR Analysis

Total RNA was extracted using E.Z.N.A. blood RNA kit (Omega, Norcross, GA) according to the manufacturer's instructions. Reverse transcription was performed with SuperScript RT II (Invitrogen, Carlsbad, CA) according to manufacturer instructions, at 42°C for 2 hours. Ribosomal 18S, glyceraldehyde-3-phosphate-dehydrogenase (GAPDH), and  $\beta$ -actin were used as reference genes. cIAP1, cIAP2, XIAP, ML-IAP, ADM, and TNF $\alpha$  transcripts were analyzed by quantitative RT-PCR using a LightCycler 480 and LightCycler 480 SYBRGreen I Master (Roche Applied Science, Meylan, France). The relative expression ratio of the target mRNA and reference RNA (18S, GAPDH,  $\beta$ -actin) was calculated using Q-PCR efficiencies and the crossing point

Cp deviation of a stem-like cell lines versus normoxic DMSO control. All determinations were performed in triplicate. Results are expressed as median. Forward and reverse primers for each gene are listed below *18S*: 5'-CTACCACATCCAAGGAAGCA-3', 5'-TTTTTCGCTCAACTACTCCCCG-3'; *GAPDH*: 5'-CAAATTCATGGCACCGTC-3', 5'-CCCCTTGATTTGGAGGA-3'; *β-actin*: 5'-CCACTGTGCCCATCTACG-3', 5'-AGGATCTTCAATGAGGTAGTCAGTCAG-3'; *cIAP1*: 5'-CTGGCCATCTAGTGTCCAG-3', 5'-TCTACCATGGATCATCTCC-3'; *cIAP2*: 5'-CTGCTATCCACATCAGACAG-3', 5'-CCAGGCTTCTACTAAAGCCC-3'; *XIAP*: 5'-GGGGTTCAGTTCAAGGAC-3', 5'-GCGCCTTAGCTGCTTTCAG-3'; *ML-IAP*: 5'-CCTGACAGAGGAGG AAGAGG-3', 5'-ACCTCACCTTGTCTGATGG-3'; *ADM*: 5'-TGCCAGACCCATTATTCGG-3', 5'-AGTTGTTTCATGCTGGCCG-3'; and *TNFα*: 5'-ACAACCTCAGACGCCACAT-3', 5'-TCCTTCCAGGGGAGAGG-3'.

### Protein Extraction and Western Blotting

Proteins were extracted with RIPA lysis buffer supplemented with protease (Roche Applied Science) and phosphatase (Santa Cruz Biotechnology, Dallas, TX, USA for phospho-proteins) inhibitors for 30 minutes on ice followed by 10 minutes centrifugation at 12,000 rpm. Fifty micrograms of proteins per lane were separated by 12% SDS-PAGE and transferred onto nitrocellulose membrane. After 1 hour of blocking in 5% skimmed milk or in tris-buffered saline (TBS)/bovine serum albumin (BSA) 5% for phospho-proteins, membranes were incubated with the following antibodies: anti-cIAP1 (0.2 µg/ml, R&D Systems, Minneapolis, MN, USA), anti-cIAP2 (0.2 µg/ml, Merck KGaA), anti-XIAP (0.25 µg/ml, clone 28, BD Biosciences), anti-ML-IAP (0.5 µg/ml, clone 88C570, Novus, St. Louis, MO, USA), anti-β-actin (1/5,000, clone AC-15, Merck KGaA), anti-Phospho-Chk1 (Ser345; 1:1,000, clone 133D3), anti-Phospho-ERK1/2 (1:2,000), anti-total-ERK1/2 (1:1,000), anti-Phospho-IκBα (1:1,000), anti-total-IκBα (1:1,000) all from Cell Signaling Technology (Danvers, MA, USA), anti-Phospho-γH2AX (Ser139; clone JBW301), anti-total-γH2AX (1:1,000, Merck KGaA) and anti-total-Chk1 (1:1,000, Abcam, Cambridge, U.K.) in TBS supplemented with 5% BSA and 0.1% Tween 20 (Sigma-Aldrich) overnight at 4°C under shaking. The following horseradish peroxidase-conjugated donkey anti-mouse IgG, goat anti-rabbit IgG (Santa Cruz Biotechnology) and rabbit anti-goat IgG (Dako France, Ullis, France) antibodies were used for proteins detection. The following fluorescent secondary antibodies were used: donkey anti-rabbit-800CW or donkey anti-mouse-680LT (LI-COR, Lincoln, NE, USA) and detected with Odyssey Clx Imaging System from LI-COR for the phospho-proteins. Quantifications were performed using ImageJ software (National Institutes of Health, Bethesda, MD) on preflashed x-ray films. Data presented were standardized on β-actin expression and for phospho-proteins, quantifications are represented by phospho-protein/total-protein ratio.

### Flow Cytometry

Anti-CD133-PE (CD133/2) and A2B5-APC antibodies were purchased by Miltenyi Biotec (Bergisch Gladbach, Germany); staining assays were performed as previously described [4]. For GFAP and Ki67 stainings, cells were harvested, fixed at room temperature in 2% paraformaldehyde for 10 minutes. Then cells were permeabilized with denaturing buffer (HCl 37%, Triton X-100, phosphate-buffered saline [PBS] 10×) for 20 minutes at 37°C and neutralized with sodium tetraborate for 10 minutes at room temperature. Cells were incubated with anti-GFAP-PE (BD Biosciences) and anti-Ki67-FITC (clone MIB1, Dako) for

30 minutes at room temperature. Cells were processed on a FACS Calibur (Becton Dickinson, Heidelberg, Germany). Data were analyzed using FlowJo software (Tree Star, Inc., Ashland, OR, USA). For the analyses of the explants the same protocol was used.

### DNA Fragmentation

Fluorescence-activated cell sorting (FACS Calibur) analysis of DNA fragmentation of propidium iodide-stained nuclei was performed as described [16].

### Immunofluorescent Staining Microscopy

Before GFAP and Ki67 staining, cells or spheres were fixed with 4% paraformaldehyde, denaturated (HCl 37%, Triton X-100, PBS 10×) for 20 minutes at 37°C and neutralized with sodium tetraborate for 10 minutes at room temperature. Primary antibodies A2B5 (mouse IgM ascite, 1:1,000, kindly provided by G. Rougon), anti-GFAP (rabbit IgG, 10 µg/ml, Dako) and anti-Ki67 (mouse IgG, clone Mib1, 5 µg/ml, Dako) were incubated for 1 hour at room temperature. For A2B5, cells were fixed after staining. Double staining assays, GFAP/Ki67 were performed by sequential incubation of primary antibodies.

For phospho-γH2AX staining, cells were fixed with 95% ethanol, 5% acetic acid for 5 minutes, and blocked with TBS/BSA 3% for 30 minutes. Primary antibody phospho-γH2AX (mouse IgG1, clone JBW301, 1:500, Merck KGaA) was incubated for 1 hour at room temperature in blocking buffer. Fluorochrome conjugated-secondary antibodies, Alexa Fluor 568 anti-mouse IgM, Alexa Fluor 568 anti-rabbit IgG and Alexa Fluor 488 anti-mouse IgG (Molecular Probes, Eugene, OR, USA) were used at 2 µg/ml and incubated for 1 hour at room temperature with Hoechst.

Images were obtained using Zeiss Lsm 800 airyscan confocal microscope. Images were processed with ImageJ software.

For explants immunostainings, primary antibodies anti-ADM (rabbit, 1:1,000, kindly provided by L'H. Ouafik) and anti-GFAP were incubated overnight at 4°C and 1 hour at room temperature, respectively. For GFAP staining, the explants were fixed with 4% paraformaldehyde for 15 minutes and permeabilized with Triton 0.3%. The secondary antibodies, Alexa Fluor 568 anti-rabbit IgG (2 µg/ml, Molecular Probes) and Alexa Fluor 488 anti-rabbit IgG (2 µg/ml, Molecular Probes) were incubated for 1 hour at room temperature. The pictures were taken using a Zeiss AXIO-Observer Z1 microscope (Carl Zeiss SAS, Marly-le-Roi Cedex, France).

### PKH67 Staining

GBM9 cells were fluorescently marked using a lipophilic dye PKH67 green Fluorescent Cell Linker Kit (Sigma-Aldrich). This staining ensures the monitoring of cell proliferation in cultures for a long period. After two washes in PBS, the cell pellet was resuspended in 1 ml of Diluent C and 1 ml of dye solution for 2 minutes. Cells were washed twice with 10 ml of medium, counted and put back in culture.

### Caspase-3 Cleavage Assay

Spheres and explants were incubated with the green fluorescent NucView 488 caspase-3 substrate for profiling caspase-3 activity in living cells (Apoptosis Assay Kit NucView 488, Biotium, Inc., CA), the day of the treatment following the manufacturer's instructions.

### Cell Viability Assay

Cells were seeded on poly-DL-ornithin-coated 96-well plates (1,500 cells per well). After 24 hours, cells were treated with serial concentrations of GDC-0152 (0.01 nM; 1 nM; 100 nM; 1  $\mu$ M; 10  $\mu$ M) in 100  $\mu$ l of cell-specific medium per well for 8 days. After treatment, 10  $\mu$ l of MTT reagent (3-[4,5-dimethylthiazol-2-yl]-diphenyl tetrazolium bromide, Sigma–Aldrich) were added to each well and plates were incubated for 4 hours at 37°C. The reduced formazan was dissolved in 100  $\mu$ l of DMSO and absorbance was measured at 562 nm with an Elx800 microplate reader (Bio-Tek, Colmar, France) and data were analyzed with the Gen5 1.09 software.

### TOF-SIMS Imaging

The time-of-flight secondary ion mass spectrometry (TOF-SIMS) analyses were performed on a TOF V spectrometer (ION-TOF GmbH, Munster, Germany) located at Tescan Analytic (Tescan Analytic SAS, Fuveau, France). This spectrometer is equipped with a bismuth liquid metal ion gun: 25 keV Bi<sup>3+</sup> clusters ions were used for all experiments and an angle of incidence of 45° with respect to the sample surface. The secondary ions were extracted at 2 keV in a single stage reflector time of flight mass spectrometer. Secondary ions were post-accelerated to 10 keV at the entrance surface of the hybrid detector, made of one single microchannel plate, followed by a scintillator and a photomultiplier. The data were acquired and processed with SurfaceLab 6.5 software (ION-TOF, GmbH, Munster, Germany). Internal mass calibration was realized using H<sup>+</sup>, H<sub>2</sub><sup>+</sup> and CH<sub>3</sub><sup>+</sup> ions in the positive ion mode and with H<sup>-</sup>, C<sup>-</sup>, CH<sup>-</sup>, CH<sub>2</sub><sup>-</sup> ions in the negative ion mode. Spheres were analyzed following the O<sup>-</sup> ions. The intensity line scan of O<sup>-</sup> ion ( $m/z = 16$ ), scanning the SIMS image of spheroid, was performed in triplicate.

### Matrix Assisted Laser Desorption Ionisation-Time of Flight (MALDI-TOF) Imaging

Spheres were embedded in Gelatin (Sigma–Aldrich) at 17.5 mg/ml and stored at –20°C until use. Frozen samples were sectioned at a thickness of 12  $\mu$ m and then thaw-mounted on an indium-tin-oxide (ITO) slide (Bruker Daltonics, MA). The sections were dried for at least 30 minutes in a desiccator. Optical images were scanned using Opticlab H850 (Plustek, Taiwan) with three teaching marks for a perfect colocalization of optical images and medium-scale integration (MSI) experiments. Sections were then covered with a 2,5-dihydroxybenzoic (2,5-DHB) matrix (Bruker Daltonics) and sprayed with TM-Sprayer (HTX Imaging, CA, USA). MALDI images were obtained using MALDI-TOF UltrafleXtreme (Bruker Daltonics). FlexImaging 3.4 software (Bruker Daltonics) was used for acquisition and SCILSlab 2016 (SCILS, Bremen, Germany) was used for visualization. The images were normalized using the Root Mean Square normalization. The accurate  $m/z$  was chosen thanks to the  $m/z$  obtained from five spots at different concentrations from 500 nM to 5  $\mu$ M of GDC-0152 also spotted on the ITO slide.

### Kinome Assay

Cells were treated for 2 hours with 1 nM of GDC-0152 or DMSO and extracted in M-PER buffer (Thermo-Scientific) containing inhibitor cocktails. Ten micrograms of total amount of protein with 100  $\mu$ M of ATP were loaded with fluorescein isothiocyanate (FITC) labeled antiphospho serine/threonine antibodies (Pamgene International B.V., Hertogenbosch, The Netherlands) on PamChip. Phosphorylation activity was tagged by a FITC-conjugated antibody and recorded with a Pamstation12 (Pamgene). Results were

analyzed with BioNavigator (Pamgene). The experiment was performed in triplicate.

### Statistical Analyses

mRNA expression values from microarrays and Q-RT-PCR results were analyzed by the nonparametric Mann–Whitney test. The nonparametric Wilcoxon test was used to analyze several parameters by comparing the effect of GDC-0152 treatment on GBM stem-like cell lines in normoxic versus hypoxic conditions compared with DMSO-treated control cell lines. All statistical tests were two-sided and the threshold for statistical significance was  $p < .05$ . Tests were conducted using the XLSTAT 2013 software (Addinsoft, Paris, France).

## RESULTS

### IAPs Distribution in Hypoxic and Nonhypoxic Areas of GBMs

Intratumoral IAPs distribution within human GBMs is not well documented. We examined whether their distribution varied between hypoxic and nonhypoxic regions of the tumors. We used immunohistochemical analysis to compare the expressions of cIAP1, cIAP2, XIAP, and ML-IAP between hypoxic areas positive for CAIX and other tumor areas of eight GBMs and did not observe variations between tumor areas (Fig. 1A). We also used Affymetrix Human Genome U133A Array published data (GDS1380/GSE2485 data set from the NCBI GEO) and the GEO2R application to compare gene expression profiles of pseudopalisading cells obtained by laser capture microdissection of nine GBMs representing the most hypoxic areas of these tumors with other tumor cells ( $n = 9$ ; Fig. 1B) [23]. There was no significant difference in IAPs mRNA expressions between palisading cells and the other tumor cells. These independent data showed that IAPs are homogeneously distributed within GBMs independently of hypoxic areas.

### In Vitro Hypoxic Conditions Reflected the Human GBMs Intratumoral Microenvironment

To find a gene whose expression could discriminate hypoxic and nonhypoxic cells, we analyzed the expressions of HIF-1 $\alpha$  target genes in the database cited earlier [23]. We found that adrenomedullin, a gene known to be overexpressed in GBMs, was significantly more expressed in palisading cells (hypoxic area) than in the other tumor cells (Fig. 1C). We verified that adrenomedullin expression level can be used as a read out of hypoxia. GBM9 stem-like cells were cultivated in hypoxia (2% O<sub>2</sub>) and compared with normoxia cultures (20% O<sub>2</sub>). After 8 days, adrenomedullin mRNA level was increased 15-fold in cells cultivated in hypoxia relative to cells cultivated in normoxia, which validated our hypoxic conditions (Fig. 1D). Then, we quantified mRNA expression levels of IAPs in the four stem-like cell lines cultivated under these conditions. We found that IAPs mRNA expression levels were not significantly different between hypoxia and normoxia conditions (Fig. 1E, Supporting Information Fig. S1A) confirming the in situ data.

### IAPs Inhibition by Smac Mimetic GDC-0152 in Hypoxia

First, we quantified IAP proteins expression levels in the four stem-like cell lines cultivated in normoxia or in hypoxia. We found that IAP proteins expression levels were not significantly

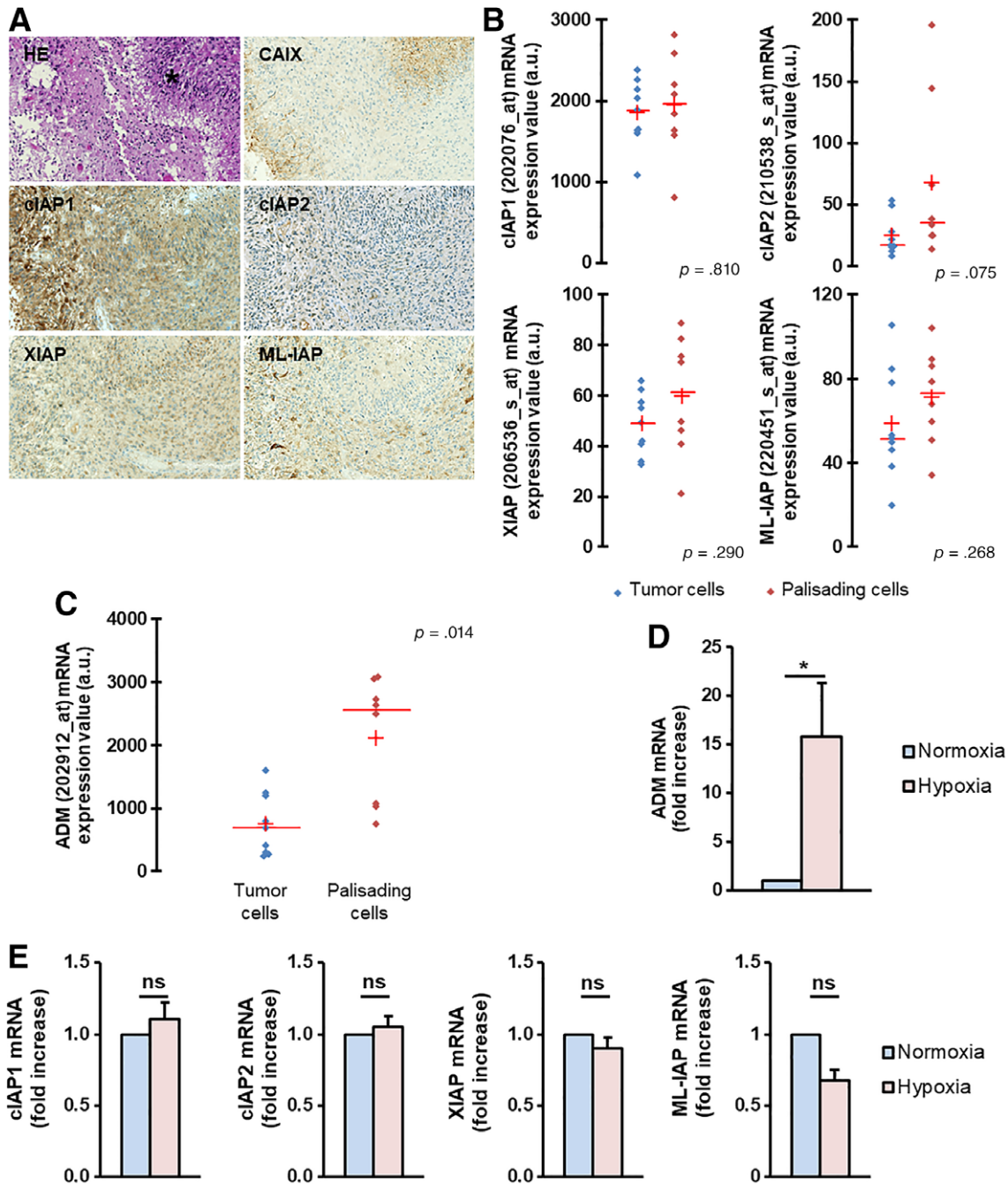


**Figure 1.** Apoptosis inhibitor proteins (IAPs) distribution between peri-necrotic and non-necrotic areas in human glioblastomas (GBMs) and set up of *in vitro* hypoxic condition. **(A):** cIAP1, cIAP2, XIAP, and ML-IAP protein expression was analyzed by immunohistochemistry on serial slides of FFPE samples from eight human GBMs. Carboxyanhydrase IX stainings highlight hypoxic areas and asterisk represents palisading cells. Pictures of a representative sample are shown. Scale bar: 100  $\mu$ m. **(B):** Scatter plots represent cIAP1, cIAP2, XIAP, and ML-IAP mRNA expression in palisading cells and common tumor cells of human GBMs. Median expression is represented by the horizontal red line and mean expression by the red cross. Data were obtained from NCBI GEO. **(C):** Adrenomedullin (ADM) mRNA was quantified in palisading cells and in common tumor cells. Median expression is represented by the horizontal red line and mean expression by the red cross. Data were obtained from NCBI GEO. **(D):** GBM9 cells were grown in monolayer in normoxia or in hypoxia for 8 days. ADM mRNA level was analyzed by Q-RT-PCR and fold increase ADM mRNA level is shown + SEM ( $n = 3$  independent experiments); \*,  $p < .05$ . **(E):** cIAP1, cIAP2, XIAP, and ML-IAP mRNA levels of GBM9 cells (grown in monolayer) were analyzed by Q-RT-PCR in normoxia or in hypoxia and fold increase mRNA levels is shown + SEM ( $n = 3$  independent experiments). Abbreviation: ns, not significant.

different between hypoxia and normoxia conditions (Supporting Information Fig. S1B).

To inhibit IAPs expression, we treated four GBM stem-like cells with Smac mimetic GDC-0152. The expression was secondly

analyzed after 8 days of GDC-0152 treatment at two concentrations already shown to be nontoxic in normoxia (0.01 nM and 1 nM) [16] (Supporting Information Fig. S2). The results showed that 1 nM GDC-0152 decreased IAPs expression in GBM stem-like

cells in hypoxia, as in normoxia. Interestingly, the four GBM stem-like cell lines tested were more sensitive to the lower concentration of GDC-0152 under hypoxia than in normoxia. For example, in the GBM9 cell line, expression of each IAP was more drastically decreased in hypoxia than in normoxia (cIAP1 was decreased 1.4-fold, XIAP 6-fold, cIAP2 1.15-fold, and ML-IAP 1.2-fold upon 0.01 nM GDC-0152). These data strongly suggested an effect of oxygen levels on the GDC-0152 mechanism of action.

### IAPs Inhibition Did Not Impair Clonogenicity of GBM Stem-like Cells in Hypoxia

We previously reported that Smac mimetics triggered GBM stem-like cell differentiation into astrocytic glial fibrillary acidic protein (GFAP)<sup>+</sup> cells when cultured in normoxia [17]. Here, we explored whether inhibiting IAPs with GDC-0152 differently alters the clonogenic potential and expression of stem-like cell markers in hypoxia in four GBM stem-like cell lines. One nanomolar GDC-0152 pretreatment significantly reduced sphere formation by all cell lines but only in normoxia: GBM6 (29%), GBM9 (38%), RNS175 (42%), and GBM40 (26%; Fig. 2A, Supporting Information Fig. S3A). Moreover, IAPs inhibition decreased A2B5 expression in all GBM stem-like cell lines (17% for GBM6; 15% for GBM9; 18% for RNS175; 5% for GBM40) and CD133 in GBM9 (46%) and GBM40 (55%) in normoxia only (Fig. 2B, 2C, Supporting Information Fig. S3B, S3C). In parallel, GDC-0152 treatment in normoxia resulted in increased numbers of GFAP<sup>+</sup> cells, which reflected more differentiated cells in three of the GBM stem-like cell lines (171% for GBM6; 44% for GBM9; 33% for RNS175), whereas it did not alter GFAP expression in hypoxia (Fig. 2D, Supporting Information Fig. S2D).

Taken together, these results demonstrated that GDC-0152 did not modify GBM stemness in hypoxia.

### IAPs Inhibition-Decreased Cell Proliferation and Increased Apoptosis Only in Hypoxia

Because we found that IAPs inhibition by GDC-0152 did not alter stem-like cell properties in hypoxia, we asked if it could affect GBM stem-like cell viability. At 0.01 nM, GDC-0152 treatment in hypoxia significantly decreased the cell viabilities of GBM6 (25%) and RNS175 (18%), and at 1 nM, the viabilities of all four GBM stem-like cell lines were affected (27.7% for GBM6; 21% for GBM9; 13.1% for RNS175; 20% for GBM40); neither concentration affected viability in normoxia (Fig. 2E, Supporting Information Fig. S2E). Because cell viability reflects the balance between proliferation and apoptosis, we quantified Ki67 expression, a marker of proliferation, and DNA fragmentation. Although in hypoxia, IAPs inhibition drastically and significantly decreased Ki67<sup>+</sup> cells in the four GBM stem-like cell lines (78% for GBM6; 64% for GBM9; 39% for RNS175, and 41% for GBM40), and in normoxia, a slight decrease in cell proliferation was quantified (Fig. 2F, 2H, Supporting Information Fig. S2F). Moreover, IAPs inhibition triggered apoptosis only in hypoxia for all GBM stem-like cell lines (56% for GBM6; 86% for GBM9; 250% for RNS175, and 172% for GBM40; Fig. 2G, 2I, Supporting Information Fig. S2G).

Altogether, these results demonstrated that IAPs inhibition altered cell viability by decreasing cell proliferation and increasing apoptosis in hypoxia.

### Validation in a 3D GBM Model

We explored oxygen levels in GBM9 spheres cultivated for 8 days in normoxia. To measure oxygen levels, we performed TOF-SIMS analyses of secondary O<sup>-</sup> ions in the spheres. The data revealed

the presence of a hypoxic core surrounded by cells more oxygenated at the periphery of the sphere (Fig. 3A). Analysis of cellular composition showed a low proportion of PKH67<sup>+</sup> proliferative cells localized in the core of the sphere (Fig. 3B). Proliferative Ki67<sup>+</sup> cells and GFAP<sup>+</sup> cells were found at the periphery of the spheres (Fig. 3C). By using MALDI images, we demonstrated that GDC-0152 can penetrate into 8-day-old spheres. The presence of GDC-0152 was confirmed by the colocalization of the [M+H]<sup>+</sup> and the [M+Na]<sup>+</sup> signal (Supporting Information Fig. S4A). This three-dimensional (3D) GBM model was therefore suitable to analyze IAPs inhibition in relation to oxygen levels.

GDC-0152 treatment of spheres resulted in a decrease in A2B5<sup>+</sup> cells of 52% and an increase in GFAP<sup>+</sup> cells of 56% (Fig. 3D). Moreover, PKH67 staining and caspase-3 cleavage quantification in the core of the GDC-0152-treated spheres revealed an increase in nonproliferative cells and induction of apoptosis, respectively, in the most hypoxic areas of the spheres (Fig. 3E). We also measured sphere diameter which reflects cellular proliferation. In all the four cell lines, sphere diameters were significantly reduced upon GDC-0152 treatment reflecting a reduction of cellular proliferation (Fig. 3E, Supporting Information Fig. S4B).

These 3D model results validated that IAPs inhibition-decreased proliferation while promoting apoptosis in the most hypoxic areas and triggered differentiation in the most oxygenated zones of the spheres.

### Differential IAPs Inhibition Effects in Human GBM Explants

To determine whether in situ human GBM tissue responds to IAPs inhibition as shown in in vitro GBM models, we performed explant cultures. First, we analyzed hypoxic areas in explants cultured both in hypoxia and in normoxia. We used adrenomedullin expression as a hypoxia read out. We found that adrenomedullin was heterogeneously expressed in normoxic explants, whereas its expression was increased in hypoxic explants (Fig. 4A). GDC-0152 treatment of explants decreased the number of A2B5<sup>+</sup> and Ki67<sup>+</sup> proliferative cells, and in contrast, increased GFAP<sup>+</sup> cells and apoptosis (Fig. 4B). Co-immunostainings were performed to search for a correlation between more differentiated cells (adrenomedullin/GFAP; Fig. 4C) and apoptotic cells (adrenomedullin/caspase-3 cleavage; Fig. 4D) with hypoxic areas. GFAP<sup>+</sup> cells did not colocalize with adrenomedullin<sup>+</sup> areas, whereas apoptotic cells were found only in hypoxic areas. These results also showed that in in situ human GBM tissues, IAPs inhibition by GDC-0152 triggered differential antitumoral effects depending on oxygen level.

### IAPs Inhibition Activated ATR-Related Signaling in Hypoxia

We showed previously that in conventional culture, herein normoxia, Smac mimetics caused stem cell differentiation depending on the NF- $\kappa$ B pathway [17]. In this study, we found that in hypoxia GDC-0152 does not induce cell differentiation but decreases proliferation and increases cell death. This suggest the involvement of other(s) intracellular signaling pathway(s), hence the importance of studying serine–threonine kinases (STK). Therefore, we performed high-throughput screening of serine–threonine kinases activity in GBM9 stem-like cells either treated with vehicle or GDC-0152 at 1 nM for 2-hour cultures either under normoxic or hypoxic conditions. Kinases involved in hypoxia response alone were removed from the analysis. We considered only the STK more activated (negative values) or less activated (positive values)

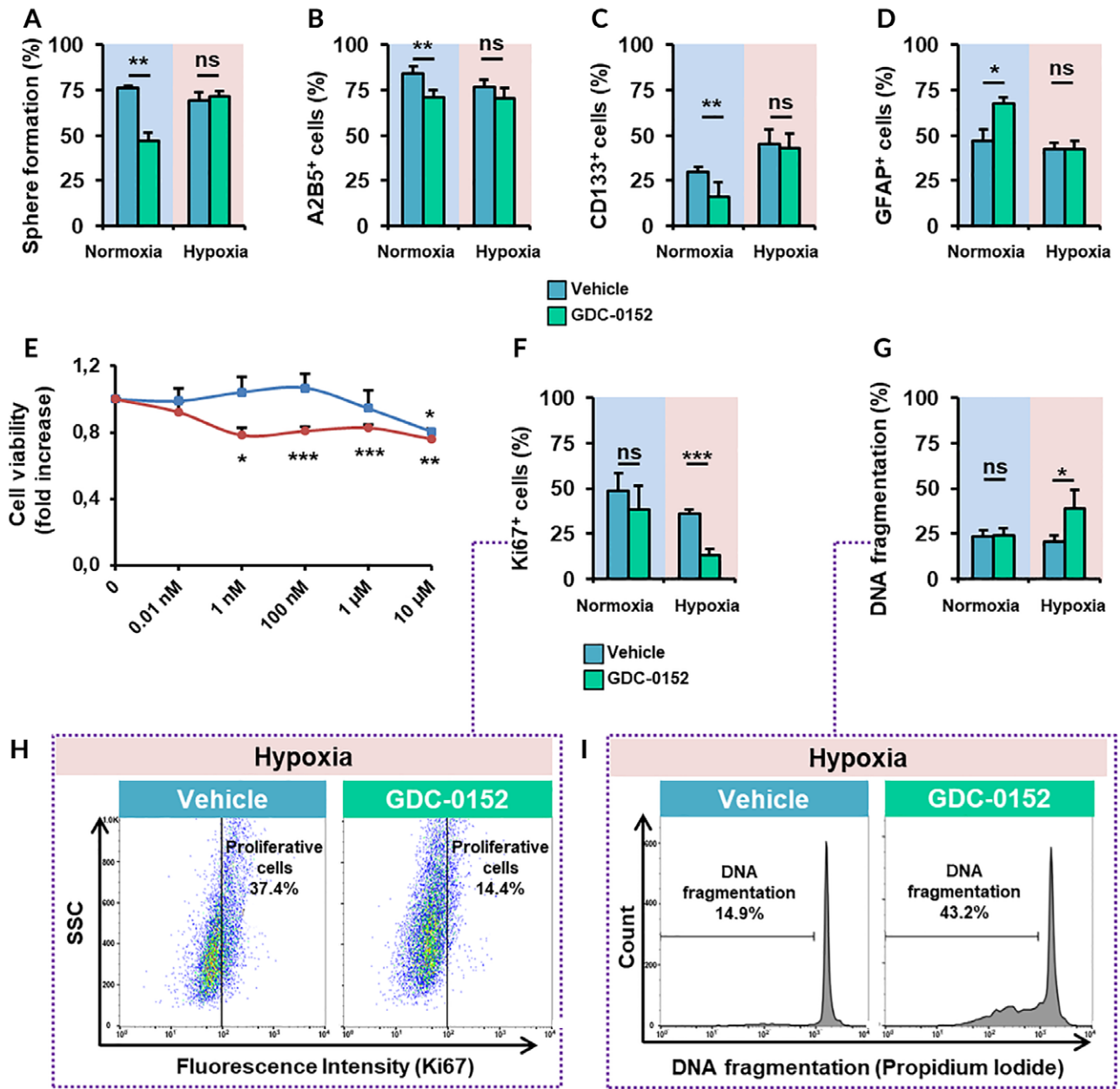


**Figure 2.** Apoptosis inhibitor proteins inhibition decreases cell proliferation and increases cell death in hypoxia. (A–D, F–I): GBM9 cells grown in monolayers and treated with vehicle alone (DMSO) or 1 nM of GDC-0152 in normoxia or in hypoxia for 8 days. (A): Percentage of self-renewal calculated as the number of spheres formed divided by the number of cells seeded. Mean + SEM ( $n = 3$  independent experiments) is shown. (B–D): After treatment, cells were dissociated and stained either with A2B5 ( $n = 8$ ), anti-CD133 ( $n = 8$ ), or anti-GFAP ( $n = 3$ ) antibodies for flow cytometry analyses. Mean + SEM. (E): GBM9 cells were treated in monolayer with increasing concentrations of GDC-0152 (0.01 nM; 1 nM; 100 nM; 1 μM; 10 μM) for 8 days in normoxia (blue) or hypoxia (red). Cell viability was expressed as fold increase of DMSO controls + SEM ( $n = 4$  in triplicate). (F): After treatment, cells were dissociated, fixed, and stained with Ki67-antibody for flow cytometry analyses and the percentage of proliferation is shown for control and GDC-0152 treated cells for normoxia or hypoxia. Data are expressed as mean + SEM ( $n = 4$ ). (G): DNA fragmentation (SubG0/G1) determined by flow cytometry for control and GDC-0152-treated cells. Data are expressed as mean + SEM ( $n = 5$ ). (H): Representative dot plots of Ki67 flow cytometry of GBM9 cells from four independent experiments. (I): Representative histograms of DNA fragmentation of GBM9 from five independent experiments. Normoxia: 20% O<sub>2</sub>; hypoxia: 2% O<sub>2</sub>; \*,  $p < .05$ ; \*\*,  $p < .01$ ; \*\*\*,  $p < .001$ ; Abbreviation: ns, not significant.

by GDC-0152 treatment (Supporting Information Fig. S5A, S5B). The MAPK, JNK, PI3K/Akt, and cell cycle pathways were found to be the most commonly represented and activated both in hypoxia and in normoxia upon GDC-0152 treatment. As expected, Smac mimetic treatment might activate the NF-κB pathway in normoxia as shown by phosphorylation of IκB kinase β (IKKβ) and ribosomal

S6 kinase 1 and 4 (RSK1,4). By contrast, we found in hypoxia that IAPs inhibition increased the phosphorylation of ATR, whereas in normoxia, the ATR pathway appeared inhibited because IAPs inhibition decreased the phosphorylation of checkpoint kinase (Chk) 1, which is the readout of ATR activity (Supporting Information Fig. S5C). The pathways potentially activated by GDC-0152

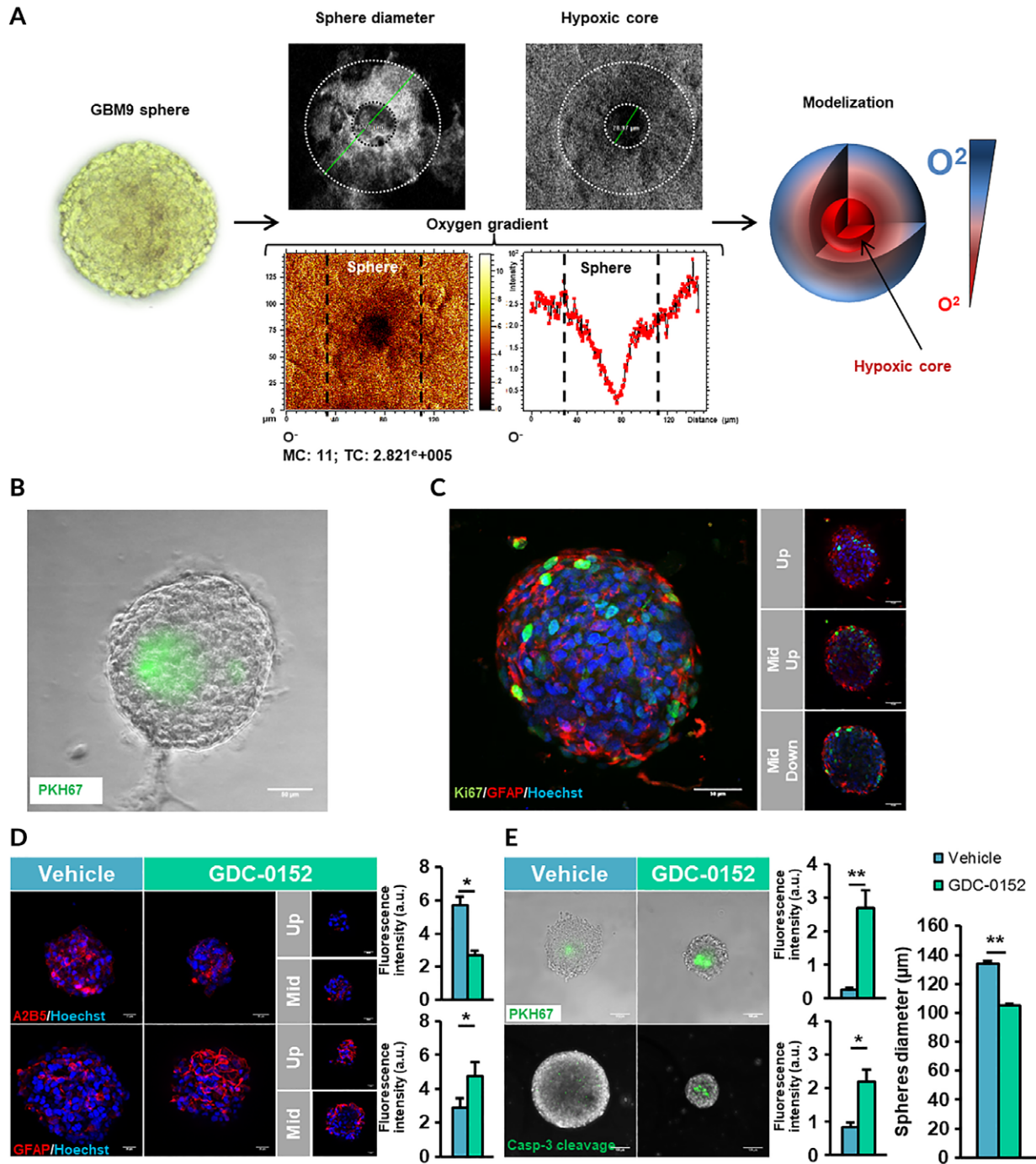


**Figure 3.** Apoptosis inhibitor proteins inhibition effects on glioblastoma (GBM) three-dimensional model according to oxygen level. (A–E): GBM9 cells were grown in suspension for 8 days in normoxia. (A): Spheres were analyzed by time-of-flight secondary ion mass spectrometry imaging. Hypoxic core diameters (left) and oxygen variations (right) were measured. The amplitude of the color scale bar corresponds to the maximum number of count (MC). TC is the sum of counts recorded in all the pixels. Experiment was performed in triplicate. A modeling of spheres is presented on the right. (B): GBM9 cells were fluorescently marked using a lipophilic dye PKH67 green Fluorescent Cell Linker Kit. Spheres were analyzed by microscopy. Scale bar: 50  $\mu\text{m}$ . (C): GFAP (red) and Ki67 (green) immunofluorescences were performed and counterstained with Hoechst. Stainings were analyzed by confocal microscopy on 15 z stacks projection. For the top of the sphere (up) 1 to 5 z were projected, for middle up 6 to 10 z, and for middle down 11 to 15 z were projected. Scale bar: 50  $\mu\text{m}$ . (B, C): Representative stainings of three independent experiments are shown. (D, E): After 8 days, cells were treated with vehicle alone (DMSO) or GDC-0152 (1  $\mu\text{M}$ ) for 8 days (sphere of 16 days). Quantification of fluorescence intensity was performed by ImageJ ( $n = 5$  spheres) and divided by the size of the sphere ( $n = 3$  independent experiments). Scale bar: 20  $\mu\text{m}$ . (D): GBM9 spheres were stained with A2B5 and anti-GFAP antibodies and counterstained with Hoechst. Representative pictures of 15 z stacks projection ( $n = 3$  independent experiments) are shown. (E): GBM9 spheres were fluorescently marked using a lipophilic dye PKH67, then green fluorescence was quantified after 8 days of treatment. To monitor apoptosis, spheres were incubated with the green fluorescent NucView 488 caspase-3 substrate for profiling caspase-3 activity in living cells. Spheres diameter represents the proliferation rate and was measured after 8 days of treatment. Mean + SEM of six independent experiments is shown; \*,  $p < .05$ ; \*\*,  $p < .01$ .

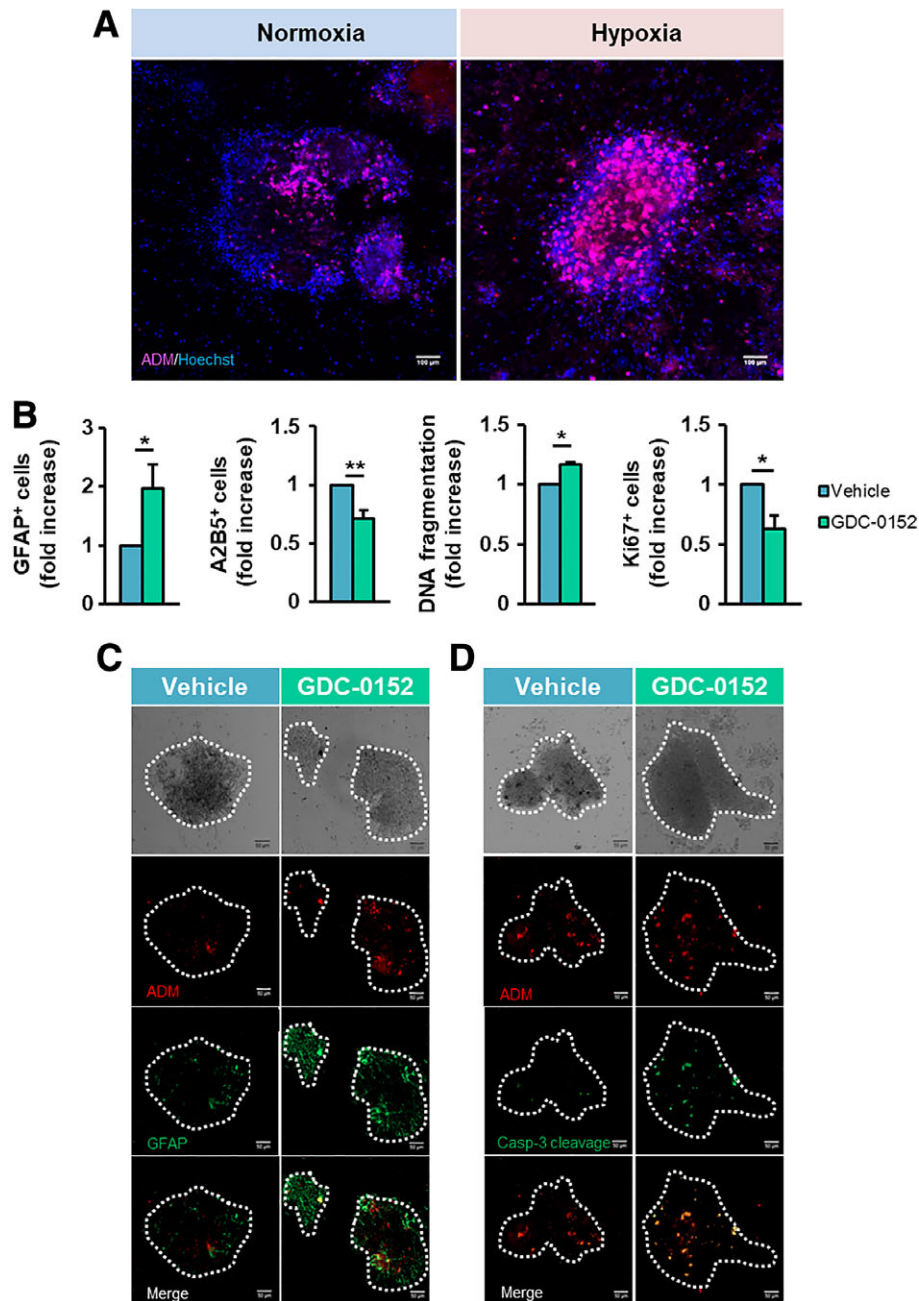


**Figure 4.** Apoptosis inhibitor effects on human glioblastoma (GBM) explants according to oxygen level. **(A):** To identify hypoxic areas, human explants were grown for 3 days in normoxia or in hypoxia. Explants were stained with anti-ADM antibody and counterstained with Hoechst. Representative stainings of two independent experiments are shown. Scale bar: 100  $\mu$ m. Normoxia: 20% O<sub>2</sub> and hypoxia: 2% O<sub>2</sub>. **(B–D):** Human explants were grown for 3 days and then treated with vehicle (DMSO) or GDC-0152 (1  $\mu$ M) for 3 days. **(B):** Quantification of GFAP, A2B5, CD133, and Ki67 positive cells in human GBM tissue samples were analyzed by flow cytometry + SEM (independent experiments, respectively,  $n = 7$ ,  $n = 9$ ,  $n = 7$ , and  $n = 6$ ). DNA fragmentation was quantified by flow cytometry ( $n = 8$ ). Data are expressed as fold increase of vehicle-treated cells + SEM. **(C):** Human explants were stained with anti-GFAP and anti-ADM antibodies. **(D):** To monitor apoptosis, viable tumor explants were incubated with the green fluorescent NucView 488 caspase-3 substrate. **(C–D):** White dotted lines delimit explants. A representative picture of three human GBM samples is shown. Scale bar: 50  $\mu$ m; \*,  $p < .05$ ; \*\*,  $p < .01$ .

according to oxygen level are represented in Figure 5A. To validate these results, we analyzed phospho-I $\kappa$ B $\alpha$ , phospho-ERK1/2, phospho-Chk1 protein expression and their respective total form in GBM9 cells (Fig. 5B), and in RNS175 and GBM40 cells (data not shown). IAPs inhibition triggered phosphorylation of I $\kappa$ B $\alpha$  only in normoxia, phosphorylation of Chk1 only in hypoxia, and phosphorylation of ERK1/2 under both conditions (Fig. 5B, 5C).

To test whether in hypoxia IAPs inhibition-decreased cell viability in an ATR-dependent manner, we used a specific inhibitor of ATR activity (ATR1) in cotreatment with GDC-0152. The results showed that in combination with ATR1, the effect of IAPs inhibition on cell viability was totally reversed (Fig. 5D). To determine whether this ATR activation was dependent of DNA damage, we analyzed  $\gamma$ H2AX-expression and phosphorylation.

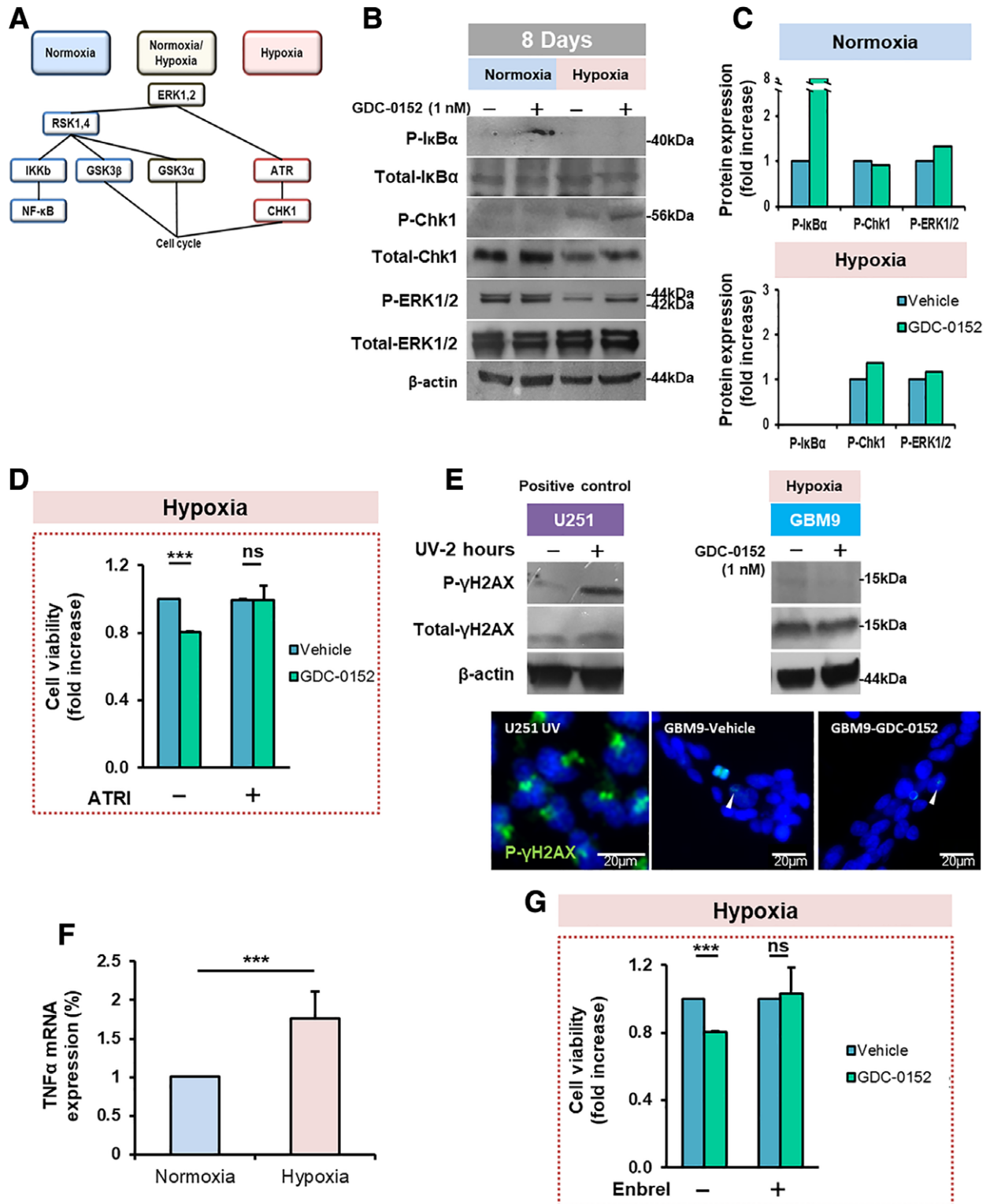


**Figure 5.** Signaling pathways involved upon apoptosis inhibitor proteins (IAPs) inhibition depending on oxygen level. **(A):** GBM9 stem-like cells were cultivated in monolayer in normoxia or hypoxia and treated with vehicle alone (DMSO) or 1 nM of GDC-0152 for 2 hours. Serine/threonine kinases activity was analyzed by PamGen kinome assay. The scheme represents the signaling pathways triggered by IAPs inhibition depending on microenvironment. **(B):** Validation of kinome results on GBM9 stem-like cells at 8 days of vehicle or 1 nM of GDC-0152 treatment in normoxia or in hypoxia. Phospho(P)-IκBα for NF-κB pathway, phospho(P)-ERK1/2 for MAPK pathway, phospho(P)-Chk1 and their total form were analyzed by Western blotting. **(C):** Quantification of Western blot analyses ( $n = 2$ ). **(D):** Cell viability of GBM9 stem like-cells cultivated in hypoxia, treated with 1 nM of GDC-0152 alone or cotreated with GDC-0152 and 10 nM of ATR inhibitor (ATRI) was measured by MTT assay and expressed as fold increase of ATRI controls + SEM ( $n = 3$  independent experiments). **(E):** U251 cells were exposed to UV irradiation for 2 hours (DNA damage positive control) and GBM9 stem-like cells were cultivated in monolayer in hypoxia (Figure legend continues on next page.)

We used U251 cell line exposed to UV irradiation as positive control and compared the phosphorylation status of  $\gamma$ H2AX in GBM9 cells treated with GDC-0152 in hypoxia (Fig. 5E). In contrast to U251 cells, we did not notice any modification of  $\gamma$ H2AX phosphorylation in treated-GBM9 cells (Fig. 5E) or in other cell lines (data not shown).

Moreover, we quantified TNF $\alpha$  mRNA expression and found that it was significantly more expressed in hypoxia than in normoxia (Fig. 5F). Then, we used the TNF $\alpha$  blocking antibody Enbrel in combination with GDC-0152. TNF $\alpha$  inhibition completely blocked the effect of IAPs inhibition on cell viability in hypoxia (Fig. 5G).

Taken together, these results demonstrated that IAPs inhibition triggered different cell signaling pathways depending on oxygen level. Hypoxia activated ATR and involved TNF $\alpha$  signaling.

## DISCUSSION

This study showed that oxygen level determined the effects of IAPs on the fate of stem-like cells in GBM. In an environment rich in oxygen, GBM stem-like cells lose their stem cell properties. In contrast, in an environment deprived of oxygen, IAPs inhibition did not affect stemness but rather cell viability by decreasing proliferation and increasing apoptosis.

We showed that these dual effects due to IAPs inhibition were driven by distinct signaling pathways, and we highlighted a novel signaling pathway involved in the Smac mimetic response. Upon oxygen deprivation, IAPs inhibition activated ATR and triggered the phosphorylation of its principal target, Chk1. Furthermore, the pharmacological inhibition of ATR blocked the effect of IAPs inhibition on cell viability. ATR, one of the main proteins involved in the DNA damage response, is essential for the maintenance of genomic integrity during a broad spectrum of DNA damages; it controls cell cycle and cell survival even in the absence of DNA damage (e.g., replicative stress; [26,27]). In the present study, ATR was activated after only 2 hours of IAPs inhibition in hypoxia, which suggested an activation independent of any DNA damage. Toledo et al. proposed a tumor-suppressive potential of ATR activation in a DNA-damage-independent manner by promoting cell cycle arrest [28]. ATR activation has also been described to trigger apoptosis, and under our conditions, ATR could be involved both in proliferation arrest and apoptosis induction [29,30]. Moreover, we showed that TNF $\alpha$  expression increased in hypoxia relative to that in normoxia and contributed to IAPs inhibition-decreased cell viability in hypoxia as evidenced by the impaired Smac mimetic effect on cell viability caused by Enbrel. TNF $\alpha$  is well known to potentiate Smac mimetics efficiency [31,32] and probably synergizes with GDC-0152 in hypoxia to trigger cell death. However, how and whether TNF $\alpha$  and ATR pathways are connected or act in parallel remains to be determined.

The cyto-architecture of GBMs is complex and covered by a gradient of oxygen. The use of GBM organoids described by

others [33] was not suitable for our purpose as the growth of organoids is slow and barely reproducible. Furthermore, the sphere model appeared especially interesting to study hypoxia as we could measure different levels of oxygen from the core to the periphery. Therefore, we characterized and used an integrated 3D GBM model to quantify, compare, and correlate IAPs inhibition effects with oxygen level. The sphere model that we set up is instrumental to analyze drug responses in terms of phenotypic remodeling, apoptosis, and proliferation in parallel with oxygen level variations.

Eradication of tumor stem cells is a major current challenge. We observed that IAPs inhibition via the use of Smac mimetic eliminated stem cells even in low oxygen level. In addition, in this study we uncovered that the Smac mimetic GDC-0152 caused a more drastic decrease in IAPs in hypoxia and at lower concentrations than those in normoxia. This is important with reference to the fact that in a hypoxic environment, cells gain stemness and become more resistant to conventional therapy. Our findings are consistent with those of Lu et al. on the Smac mimetic AT-406 in cervical cancer. They showed that upon AT-406 treatment, cells were more sensitive to radiation in hypoxia than in normoxia and that cIAP1 and XIAP degradation was increased in hypoxia [34]. These results support the implication of a direct endogenous IAP protein antagonist that could be downregulated in hypoxia similarly to Smac or deubiquitinases [35–37]. Importantly, we confirmed the effect of hypoxia on the Smac mimetic GDC-0152 resulting effects in human GBM tissue.

## CONCLUSION

Hypoxia is a major cause of treatment resistance in solid cancer. Therefore, the identification of this dual role of IAPs, and thereby of Smac mimetics, is of high interest clinically, in particular to target stem cells located in hypoxic areas of solid tumors.

## ACKNOWLEDGMENTS

This study was supported by Institut National du Cancer (grants INCa-DGOS-INSERM 6038 and PLBIO N°2014-165), Cancéropôle PACA and institutional grants (INSERM, Aix-Marseille University). A.S. is supported by the Association pour la Recherche sur les Tumeurs Cérébrales (ARTC-Sud). We thank P. Weber for confocal microscopy support, L. Dubrez-Daloz, C. Delfino, and N. Mazure for technical advices and R. Pruss for proof reading and suggestions.

## AUTHOR CONTRIBUTIONS

A.S.: conception and design, collection and assembly of data, data analysis and interpretation, manuscript writing, final approval of manuscript; J.C., M.C., J.R., and N.B.-K.: collection of data; C.N.: collection and assembly of data; C.C.: data analysis; D.L., H.K., and V.Q.: provision of study material; G.R.: manuscript writing, final approval of manuscript; D.F.-B.: conception, manuscript writing,

(Figure legend continued from previous page.)

hypoxia and treated with vehicle alone (DMSO) or 1 nM of GDC-0152 for 2 hours. Phospho(P)- $\gamma$ H2AX and total- $\gamma$ H2AX were analyzed by Western blotting and P- $\gamma$ H2AX (green) was also analyzed by immunofluorescent staining microscopy, nuclei are in blue. A representative picture of three experiments is shown. Scale bar: 20  $\mu$ m. (F): TNF $\alpha$  mRNA level was analyzed by Q-RT-PCR and fold increase TNF $\alpha$  mRNA level is shown + SEM ( $n = 3$  independent experiments). (G): Cell viability of GBM9 cells cultivated in hypoxia, treated with 1 nM of GDC-0152 alone or cotreated with GDC-0152 and 25  $\mu$ g/ml of Enbrel (TNF $\alpha$  blocking antibody) was measured by MTT assay and expressed as fold increase of Enbrel controls + SEM ( $n = 4$  independent experiments). Each experiment was performed in triplicate; \*\*\*,  $p < .001$ . Abbreviation: ns, not significant.

final approval of manuscript; A.T.: conception and design, collection and assembly of data, data interpretation, manuscript writing, final approval of manuscript.

#### DISCLOSURE OF POTENTIAL CONFLICTS OF INTEREST

The authors indicated no potential conflicts of interest.

#### REFERENCES

- 1 Soeda A, Park M, Lee D et al. Hypoxia promotes expansion of the CD133-positive glioma stem cells through activation of HIF-1 $\alpha$ . *Oncogene* 2009;28:3949–3959.
- 2 Singh SK, Hawkins C, Clarke ID et al. Identification of human brain tumour initiating cells. *Nature* 2004;432:396–401.
- 3 Colin C, Baeza N, Tong S et al. In vitro identification and functional characterization of glial precursor cells in human gliomas. *Neuropathol Appl Neurobiol* 2006;32:189–202.
- 4 Tchoghandjian A, Baeza N, Colin C et al. A2B5 cells from human glioblastoma have cancer stem cell properties. *Brain Pathol* 2010;20:211–221.
- 5 Tchoghandjian A, Baeza-Kallee N, Beclin C et al. Cortical and subventricular zone glioblastoma-derived stem-like cells display different molecular profiles and differential in vitro and in vivo properties. *Ann Surg Oncol* 2012;19:5608–5619.
- 6 Fulda S, Vucic D. Targeting IAP proteins for therapeutic intervention in cancer. *Nat Rev Drug Discov* 2012;11:109–124.
- 7 Feltham R, Khan N, Silke J. IAPs and ubiquitylation. *IUBMB Life* 2012;64:411–418.
- 8 Varfolomeev E, Goncharov T, Fedorova AV et al. c-IAP1 and c-IAP2 are critical mediators of tumor necrosis factor  $\alpha$  (TNF $\alpha$ )-induced NF- $\kappa$ B activation. *J Biol Chem* 2008;283:24295–24299.
- 9 Bertrand MJM, Milutinovic S, Dickson KM et al. cIAP1 and cIAP2 facilitate cancer cell survival by functioning as E3 ligases that promote RIP1 ubiquitination. *Mol Cell* 2008;30:689–700.
- 10 Vallabhapurapu S, Matsuzawa A, Zhang W et al. Nonredundant and complementary functions of TRAF2 and TRAF3 in a ubiquitination cascade that activates NIK-dependent alternative NF- $\kappa$ B signaling. *Nat Immunol* 2008;9:1364–1370.
- 11 Zarnegar BJ, Wang Y, Mahoney DJ et al. Noncanonical NF- $\kappa$ B activation requires coordinated assembly of a regulatory complex of the adaptors cIAP1, cIAP2, TRAF2 and TRAF3 and the kinase NIK. *Nat Immunol* 2008;9:1371–1378.
- 12 Varfolomeev E, Blankenship JW, Wayson SM et al. IAP antagonists induce autoubiquitination of c-IAPs, NF- $\kappa$ B activation, and TNF $\alpha$ -dependent apoptosis. *Cell* 2007;131:669–681.
- 13 Vince JE, Wong WW-L, Khan N et al. IAP antagonists target cIAP1 to induce TNF $\alpha$ -dependent apoptosis. *Cell* 2007;131:682–693.
- 14 Tchoghandjian A, Jennewein C, Eckhardt I et al. Identification of non-canonical NF- $\kappa$ B signaling as a critical mediator of Smac mimetic-stimulated migration and invasion of glioblastoma cells. *Cell Death Dis* 2013;4:e564.
- 15 Flygare JA, Beresini M, Budha N et al. Discovery of a potent small-molecule antagonist of inhibitor of apoptosis (IAP) proteins and clinical candidate for the treatment of cancer (GDC-0152). *J Med Chem* 2012;55:4101–4113.
- 16 Tchoghandjian A, Soubéran A, Tabouret E et al. Inhibitor of apoptosis protein expression in glioblastomas and their in vitro and in vivo targeting by SMAC mimetic GDC-0152. *Cell Death Dis* 2016;7:e2325.
- 17 Tchoghandjian A, Jennewein C, Eckhardt I et al. Smac mimetic promotes glioblastoma cancer stem-like cell differentiation by activating NF- $\kappa$ B. *Cell Death Differ* 2014;21:735–747.
- 18 Dong Z, Venkatachalam MA, Wang J et al. Up-regulation of apoptosis inhibitory protein IAP-2 by hypoxia. Hif-1-independent mechanisms. *J Biol Chem* 2001;276:18702–18709.
- 19 Yang W, Cooke M, Duckett CS et al. Distinctive effects of the cellular inhibitor of apoptosis protein c-IAP2 through stabilization by XIAP in glioblastoma multiforme cells. *Cell Cycle Georget Tex* 2014;13:992–1005.
- 20 Hsieh C-H, Lin Y-J, Wu C-P et al. Livin contributes to tumor hypoxia-induced resistance to cytotoxic therapies in glioblastoma multiforme. *Clin Cancer Res* 2015;21:460–470.
- 21 Edgar R, Domrachev M, Lash AE. Gene expression omnibus: NCBI gene expression and hybridization array data repository. *Nucleic Acids Res* 2002;30:207–210.
- 22 Barrett T, Wilhite SE, Ledoux P et al. NCBI GEO: Archive for functional genomics data sets—Update. *Nucleic Acids Res* 2013;41:D991–D995.
- 23 Dong S, Nutt CL, Betensky RA et al. Histology-based expression profiling yields novel prognostic markers in human glioblastoma. *J Neuropathol Exp Neurol* 2005;64:948–955.
- 24 Verhaak RGW, Hoadley KA, Purdom E et al. Integrated genomic analysis identifies clinically relevant subtypes of glioblastoma characterized by abnormalities in PDGFRA, IDH1, EGFR, and NF1. *Cancer Cell* 2010;17:98–110.
- 25 Wang Q, Hu B, Hu X et al. Tumor evolution of glioma-intrinsic gene expression subtypes associates with immunological changes in the microenvironment. *Cancer Cell* 2017;32:42.e6–56.e6.
- 26 Murga M, Bunting S, Montaña MF et al. A mouse model of the ATR-Seckel Syndrome reveals that replicative stress during embryogenesis limits mammalian lifespan. *Nat Genet* 2009;41:891–898.
- 27 Shiotani B, Nguyen HD, Håkansson P et al. Two distinct modes of ATR activation orchestrated by Rad17 and Nbs1. *Cell Rep* 2013;3:1651–1662.
- 28 Toledo LI, Murga M, Gutierrez-Martinez P et al. ATR signaling can drive cells into senescence in the absence of DNA breaks. *Genes Dev* 2008;22:297–302.
- 29 Wei L, Zhu S, Wang J et al. Induction of a cellular DNA damage response by porcine circovirus type 2 facilitates viral replication and mediates apoptotic responses. *Sci Rep* 2016;6:39444.
- 30 García V, Lara-Chica M, Cantarero I et al. Galiellalactone induces cell cycle arrest and apoptosis through the ATM/ATR pathway in prostate cancer cells. *Oncotarget* 2015;7:4490–4506.
- 31 Beug ST, Beauregard CE, Healy C et al. Smac mimetics synergize with immune checkpoint inhibitors to promote tumour immunity against glioblastoma. *Nat Commun* 2017;8.
- 32 Lalaoui N, Hänggi K, Brumatti G et al. Targeting p38 or MK2 enhances the anti-leukemic activity of Smac-mimetics. *Cancer Cell* 2016;29:145–158.
- 33 Hubert CG, Rivera M, Spangler LC et al. A three-dimensional organoid culture system derived from human glioblastomas recapitulates the hypoxic gradients and cancer stem cell heterogeneity of tumors found in vivo. *Cancer Res* 2016;76:2465–2477.
- 34 Lu J, Qin Q, Zhan L-L et al. AT-406, an IAP inhibitor, activates apoptosis and induces radiosensitization of normoxic and hypoxic cervical cancer cells. *J Pharmacol Sci* 2014;126:56–65.
- 35 Guo J, Shinriki S, Su Y et al. Hypoxia suppresses cylindromatosis (CYLD) expression to promote inflammation in glioblastoma: Possible link to acquired resistance to anti-VEGF therapy. *Oncotarget* 2014;5:6353–6364.
- 36 Lee E-W, Song J. USP11: A key regulator of cIAP2 stability and sensitivity to SMAC mimetics. *Mol Cell Oncol* 2015;3.
- 37 Engel K, Rudelius M, Slawska J et al. USP9X stabilizes XIAP to regulate mitotic cell death and chemoresistance in aggressive B-cell lymphoma. *EMBO Mol Med* 2016;8:851–862.



See [www.StemCells.com](http://www.StemCells.com) for supporting information available online.